MRDC41092.35FR
NASA CR-168099

MRDC41092.35FR
NASA CR-168099
Copy No. 60

GROWTH AND CHARACTERIZATION OF CZOCHRALSKI-GROWN n- AND p-TYPE GaAs FOR SPACE SOLAR CELL SUBSTRATES

FINAL REPORT FOR THE PERIOD
May 29, 1981 through May 28, 1982

CONTRACT NO. NAS3-22235

Prepared for

National Aeronautics and Space Administration
Lewis Research Center
21000 Brookpark Road
Cleveland, OH 44135

R.T. Chen
Principal Investigator

JUNE 1983

Rockwell International

1. Report No.	2. Government Accession No.	3. Recipient's Catalog No.
CR-168099		

4. Title and Subtitle	5. Report Date
Growth and Characterization of Czochralski-grown n- and p-type GaAs for Space Solar Cell Substrates	JUNE 1983
	6. Performing Organization Code
7. Author(s)	8. Performing Organization Report No.
R. T. Chen	MRDC 41092.35FR
	10. Work Unit No.
9. Performing Organization Name and Address	
Rockwell International Microelectronics Research and Development Center 1049 Camino Dos Rios Thousand Oaks, CA 91360	11. Contract or Grant No. NAS3-22235
	13. Type of Report and Period Covered Final Report for period 5/29/81 through 5/28/82
12. Sponsoring Agency Name and Address	
NASA Lewis Research Center Cleveland, Ohio 44135	14. Sponsoring Agency Code 4231

15. Supplementary Notes

16. Abstract

Progress in LEC (liquid encapsulated Czochralski) crystal growth techniques for producing high-quality, 3-inch-diameter, n- and p-type GaAs crystals suitable for solar cell applications is described. The LEC crystals with low dislocation densities and background impurities, high electrical mobilities, good dopant uniformity, and long diffusion lengths were reproducibly grown through control of the material synthesis, growth and doping conditions. The capability for producing these large-area, high-quality substrates should positively impact the manufacturability of highly efficiency, low cost, radiation-hard GaAs solar cells.

17. Key Words (Suggested by Author(s))	18. Distribution Statement
LEC, GaAs, Czochralski, doped substrates, high purity, dislocation density.	Approved for public release. Distribution unlimited.

19. Security Classif. (of this report)	20. Security Classif. (of this page)	21. No. of Pages	22. Price*
Unclassified	Unclassified	45	

* For sale by the National Technical Information Service Springfield Virginia 22161

TABLE OF CONTENTS

PRECEDING PAGE BLANK NOT FILMED

LIST OF FIGURES

LIST OF FIGURES

LIST OF TABLES

1.0 INTRODUCTION

To achieve successful implementation of highly efficient, radiation hard, low-cost GaAs solar cells, the development of high quality, large diameter GaAs substrates is essential. In the past, GaAs was available only in irregular shapes and dimensions. Recent advances in GaAs bulk crystal growth related to the development of the Liquid Encapsulated Czochralski (LEC) technique have made it possible to grow large-diameter ingots. With the support of NASA in our previous program "Preparation of High Purity Low Dislocation GaAs Single Crystals" program (NAS3-22224), we improved LEC crystal growth techniques, achieving significant reductions in twinning, background impurities, and dislocation densities in 3-in. diameter undoped LEC crystals.

The purpose of the "Growth and Characterization of Czochralski-Grown n- and p-type GaAs for Space Solar Cell Substrates" program (NAS3-22235) was to build upon the techniques developed in the previous NASA program and Rockwell IR&D programs to further advance the LEC crystal growth technology to produce n- and p-type, large diameter GaAs crystals of high quality, suitable for solar cell applications. Attention was focused on materials properties important to solar cells, including the dislocation density, microstructure, background impurities, dopant uniformity, mobility, and minority carrier diffusion length. We investigated the dependence of these critical materials properties on the materials synthesis, and growth and doping conditions in order to optimize the crystal growth conditions for producing high quality solar cell substrate materials. The results were compared with those from GaAs crystals grown by conventional bulk growth techniques.

Five crystal growth experiments were performed at the Microelectronics Research and Development Center (MRDC) during the course of the program. Figure 1 shows a 2.4 Kg, Se-doped, 3-in. diameter LEC GaAs ingot (R45) grown under the program, in which the excellent diameter control ($\lesssim \pm 2$ min) has been achieved. Information concerning the growth processes, and physical and electrical characteristics for these intentionally-doped LEC ingots

MRDC82-20367

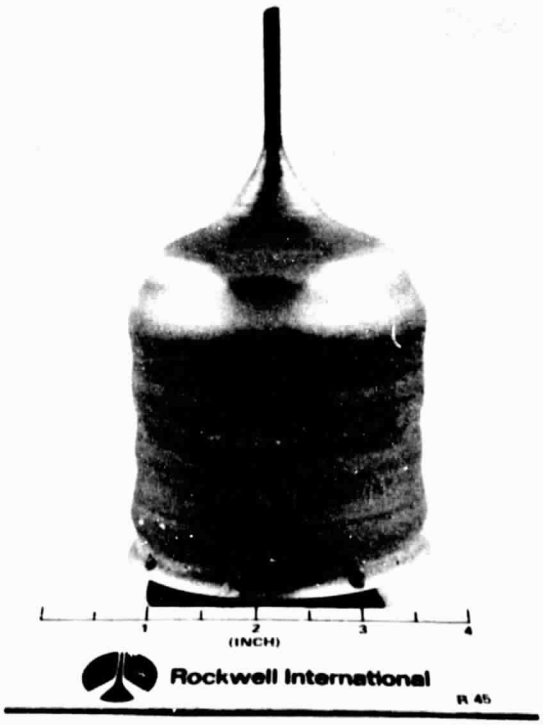

Fig. 1 Three inch diameter Se-doped LEC GaAs crystal (R45/M) grown on NASA program. The tolerance of the diameter control is better than ± 2 millimeters.

(3 n-type and 2 p-type) are summarized in Table 1. The results show that considerable progress was made during the program with respect to minimizing the concentration of background impurities, increasing mobility and minority carrier diffusion lengths, and minimizing the dislocation density. In most of these crystals, the background impurities concentration ($N_D + N_A$) and the dislocation density were lower than 1×10^{16} cm^{-3} and 1.5×10^{4} cm^{-2}, respectively. Furthermore, the dislocation density in selected areas of some crystals was lower than the 5000 cm^{-2} level. These values are the lowest reported for 3-in. doped LEC crystals. Good minority carrier diffusion lengths, as high as 1.4 μm in one of these doped crystals were also observed; however, the diffusion length up to 5.3 μm could be obtained in the p-type undoped LEC GaAs grown from the Ga-rich melt. This result will be discussed later in this report. In addition, the radial dopant distribution across 3-in. diameter wafers was below ± 10% variations in most of the crystals. These overall properties are comparable, if not superior to those of commercial Bridgman material.

As a result of the progress attained during the NASA program, we, at MRDC, are now capable of reproducibly growing large, 3-in. diameter, (100) doped LEC GaAs single crystals with high purity, low dislocation density, high mobility, radial uniformity, and long minority carrier diffusion length. This capability is an extremely encouraging development for GaAs solar cell technology, since these high quality, large-area substrate materials will provide an excellent foundation for the production of efficient, cost-effective solar cells.

In this report, experimental results obtained on the NASA "Growth and Characterization of Czochralski-Grown n- and p-type GaAs for Space Solar Cell Substrates" program are presented and discussed. In Section 2.0, the materials synthesis, growth and doping techniques are outlined. In Section 3.0, the various techniques used to characterize the lattice defects, background impurities, and electrical properties are discussed. The cause-effect relationships between the crystal growth process and material properties are discussed in Section 4.0 The results are summarized and evaluated with respect to solar cell applications in the last section.

Table 1

Summary of Physical and Electrical Characteristics of LEC GaAs Crystals Grown on Contract NAS3-22235

Rockwell I.D. No.	Crucible Material	Orientation	Dopant	Crystal Diameter (mm)	Crystal Length (cm)	Crystal Weight (kg)	$N_D + N_A$ (cm^{-3})	Free Carrier Density (cm^{-3})	Mobility ($cm^2/V\text{-}s$)	Minority Carrier Diffusion Length (μm)	EPD at Full Diameter (cm^{-2})
43	SiO_2	<100>	Si	79.4 ± 3.2	11	2.3	7×10^{15}	$0.6\text{-}1.8 \times 10^{18}$	$1.8\text{-}2.4 \times 10^3$	1.3	1.5×10^4
45	SiO_2	<100>	Se	80.0 ± 1.8	12	2.4	8×10^{15}	$0.6\text{-}1.2 \times 10^{17}$	$4.0\text{-}4.1 \times 10^3$	1.4	9.0×10^3
47	SiO_2	<100>	Se	-	17	2.2	1.4×10^{16}	$2.6\text{-}3.3 \times 10^{18}$	$1.6\text{-}1.9 \times 10^3$	0.5	1.4×10^4
48	SiO_2	<100>	Zn	82.4 ± 5.5	11	1.7	-	6.2×10^{18}	90	0.7	3.0×10^4
50	SiO_2	<100>	Zn	79.0 ± 4.3	12	2.2	1.3×10^{16}	$3.7\text{-}6.4 \times 10^{17}$	180-210	0.6	1.3×10^4

2.0 MATERIALS SYNTHESIS, GROWTH AND DOPING TECHNIQUES

In this section, the processes involved in the materials synthesis, growth and doping of LEC GaAs are described.

2.1 Growth Configuration

All crystals were grown in Rockwell International's Melbourn high-pressure LEC system at the Thousand Oaks MRDC laboratory. The configuration of the LEC system, shown schematically in Fig. 2, consists of a GaAs melt contained in either a high purity, 6 inch diameter quartz (Metals Research) or pyrolytic boron nitride (Union Carbide) crucible. The boric oxide (B_2O_3) encapsulant floats on the top surface of the melt. In addition, a thin film of B_2O_3 coats the entire surface of the crucible due to the high-temperature wetting characteristics of the materials. The B_2O_3 also wets the growing crystal. Thus, the GaAs melt is completely sealed, suppressing As evaporation and shielding the melt against contamination from the crucible and the growth ambient.

2.2 Growth Process

The major steps in the crystal growth operation included loading of the charge, heat-up, synthesis, equilibration, seeding, necking, cone growth, and pulling of the full-diameter ingot. The crucible was loaded with approximately 1400 g 6-9's Ga (Ingal International), 1500 g 6-9's As (Cominco), and a 500 g preformed B_2O_3 disk (Puratronic) with a known moisture content (typically $[H_2O] < 500$ ppm) as shown in Fig. 3. Ga, which is solid to just above room temperature, was loaded on top of the As so that the liquid Ga served to encapsulate the As. Starting with a chamber pressure of 600 psi, the crucible was heated to between 450 and 500°C, at which point the B_2O_3 melted, flowed over the charge of Ga and As, and sealed at the crucible wall. The synthesis reaction ($Ga_{liquid} + As_{solid} = GaAs_{solid}$) occurred at about 800°C. The presence of the B_2O_3 and the use of high overpressures (~ 1000 psi) prevented

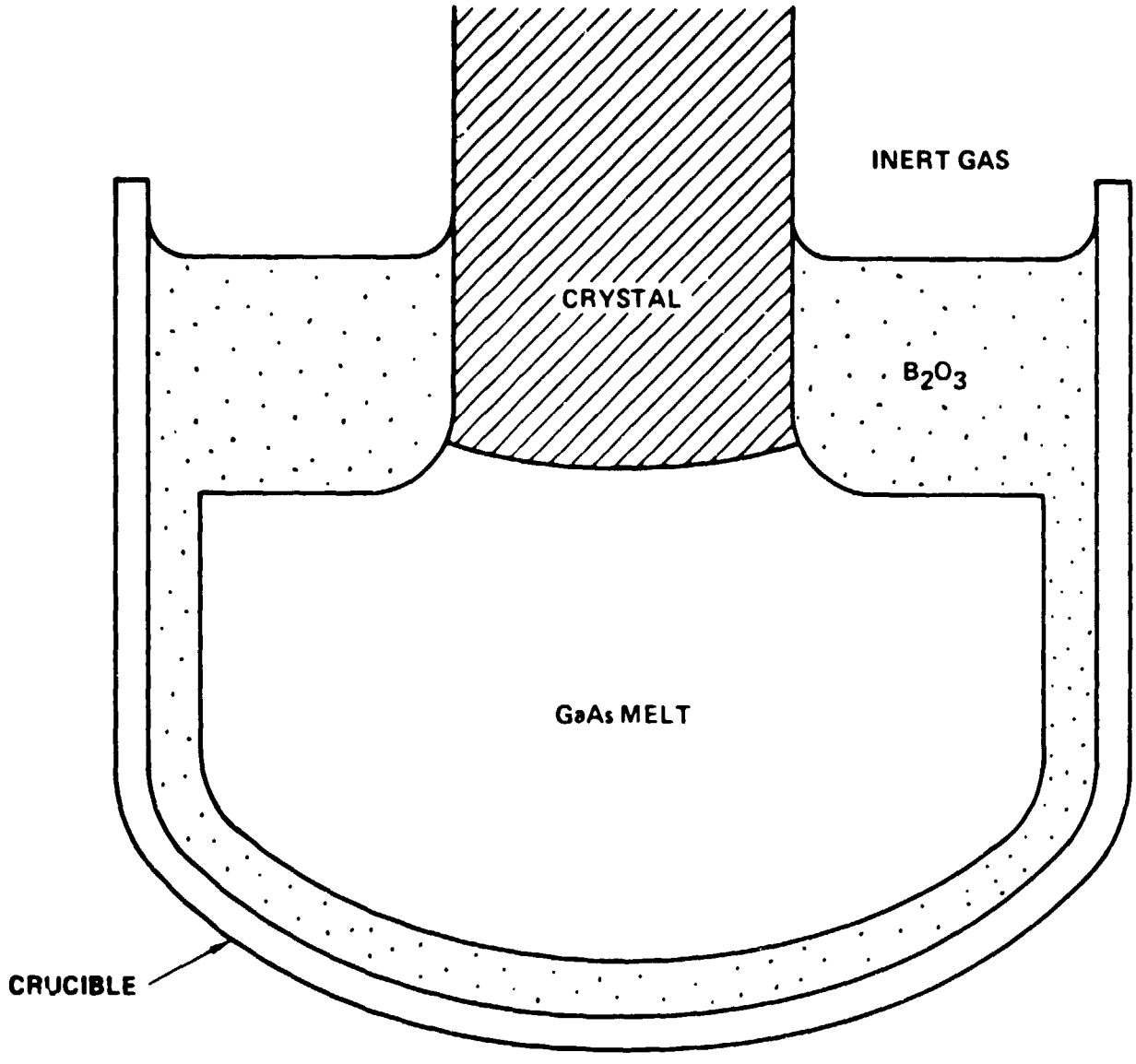

Fig. 2 Cross section of the crucible for the LEC growth system showing the location of the B_2O_3 during growth.

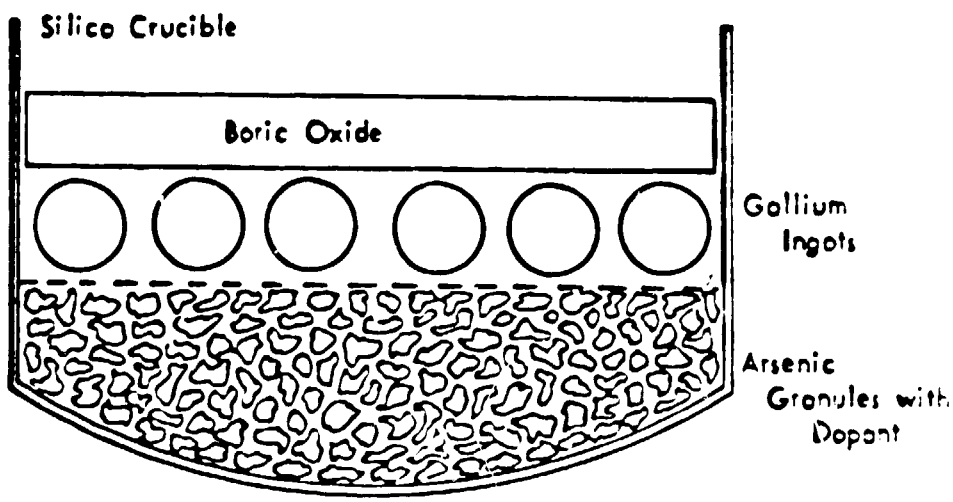

Fig. 3 Cross section of the LEC crucible before growth showing the charge of elemental Ga and As and the preformed B_2O_3 disc.

significant loss of As due to sublimination during and subsequent to synthesis. The melt was then equilibrated at the starting temperature and the growth procedure begun.

Growth was initiated by dipping the seed, which was held on the pull shaft, through the B_2O_3 and into the melt. The crystal was grown by gradually withdrawing the seed from the melt. At first, the diameter of the crystal was reduced to be below that of the seed. This procedure is referred to as Dash-type seed necking. The diameter was then allowed to expand controllably, forming the "cone". Expansion was terminated at the shoulder, and the diameter of the crystal was held constant for the remainder of the growth process, forming the "body". The shallow 30° cone was grown in all crystals (the cone angle is defined as the angle between the surface of the cone to the plane perpendicular to the growth direction.)

The diameter of the crystal was controlled by manual operation by monitoring the differential weight signal. This signal was obtained from the "load cell", a special weighing device on which the crystal and pull shaft are mounted in the LEC system. An increase or decrease of the differential weight indicates a corresponding increase or decrease in the diameter. The crystal diameter was controlled by varying the heater temperature and the cooling rate in response to changes in the differential weight signal.

The crystals were grown in the <100> direction. The weight ranged from 2.2 to 2.4 kg. The ambient pressure (argon) during growth was typically 300 psi. The seed and crucible were both rotated counter-clockwise at 6 and 15 rpm, respectively.

2.3 Doping Methods

The choice of dopants for a particular crystal growth depends on a number of factors ranging from the ultimate application of the material in a device to the specific physical-chemical conditions in the crystal growth apparatus. The dopants chosen for LEC growth of n-type and p-type GaAs should meet the criteria of low segregation coefficient (i.e., $k_o < 1$), low self-

compensation, and high physical stability (e.g., low vapor pressure). Zone-refined Si and high purity Ga_2Se_3 were used as sources of Si and Se dopants for n-type material, and p-type material was obtained by doping with Zn as Zn_3As_2. The carrier density ranged from 1×10^{17} to 1×10^{19} cm^{-3}. Super dry B_2O_3 ($[H_2O] < 150$ ppm) was used in Si-doping growth to increase its doping efficiency. Very low carrier density n- and p-type ingots were grown under the previous NASA contract (No. NAS3-22224). N-type doping below 1×10^{17} cm^{-3} was achieved without adding doping by controlling the Si incorporation resulting from the reaction of the quartz crucible with somewhat wetter B_2O_3 encapsulants (e.g., $[H_2O] < 500$ ppm). The p-type LEC GaAs crystals[2,3] with hole concentrations around $\sim 1 \times 10^{16}$ cm^{-3} were grown from undoped Ga-rich melts using a PBN crucible.

3.0 CHARACTERIZATION TECHNIQUES

This section briefly reviews the analytical techniques used to characterize the LEC GaAs material in terms of lattice defects, chemical impurities and electrical properties.

3.1 Lattice Defects

The following is a list of brief descriptions of techniques used to characterize lattice defects in the LEC material, including dislocations, twins, dislocation loops, stacking faults, interface striations and inclusions, etc.

3.1.1 Preferential Chemical Etching

The crystalline perfection of the LEC crystals was evaluated by determining the density and distribution of dislocations. Dislocations act as recombination centers and reduce the minority-carrier lifetime. The dislocation densities of (100) wafers were measured by etching polished wafers in KOH for 25 min at 400°C. This etch preferentially attacks dislocations that intersect the surface of the wafer. The density of etch pits (EPD) corresponds directly to the density of dislocations.

3.1.2 Transmission Electron Microscopy (TEM)

TEM measurements were used to examine the microstructures of the doped LEC GaAs crystals. A chemical jet etching technique using 10 HCl:1 H_2O_2:1 H_2O etching solution was applied to produce TEM thin foil with thickness less than 4000 A. The thin foils were then examined by a Philips EM-300 microscope operated at 100 kV.

3.1.3 Infrared (IR) Microscopy

Since GaAs is known to be transparent to infrared light, a microscope using the infrared light source can be used to examine lattice defects. In

this study, the IR microscope was used to examine precipitates, Ga-inclusions, doping striations, and dislocations in both n- and p-type LEC GaAs samples.

3.2 Impurity Characterization

The Secondary Ion Mass Spectrometry (SIMS) technique was used to analyze background impurities in the doped LEC materials. SIMS measurements were made at Charles Evans and Associates, San Mateo, CA. This is a chemically specific micro-analytical technique particularly well suited for transition metals and shallow donors in GaAs. The system is calibrated against ion implanted standards. The typical background detection sensitivity (the concentration below which measurements are not meaningful) of the impurities analyzed during this program are given in Table 2. Although the detection sensitivity is very low for impurities given in the table, making SIMS an excellent tool for the characterization of GaAs, the measured impurity concentration of an element in LEC GaAs is often close to the background sensitivity. Since the background sensitivity can vary from day to day (as indicated in the table), the background sensitivity was checked against a high purity standard before these analyses were made.

Table 2

Typical Background Detection Sensitivity of Impurities Detected in LEC GaAs

Element	Si	S	Se	Te	B	Mg	Cr	Mn	Fe
Background Detection Sensitivity (cm^{-3})	3E14-1E15	2-8E14	3E12	3E13	5E13-5E14	1-2E14	1-5E14	3E14-1E15	1-5E15

3.3 Electrical Measurements

Hall effect measurements and Electron Beam Induced Current (EBIC) measurements by Scanning Electron Microscopy (SEM) were used to determine electrical properties for n- and p-type LEC GaAs crystals.

3.3.1 Hall Effect Measurements

The free carrier concentration and mobility for n- and p-type LEC GaAs crystals were determined by Hall effect measurements at room temperature using Van der Pauw technique. The samples with a typical size of 7 mm × 7 mm were cut from the cone top, front, middle and tail wafers along the LEC crystals. GaInZn (or AuZn) and InSn alloys were used for ohmic contacts on p- and n-type samples, respectively. The radial carrier concentration distributions on the 3 inch diameter wafers were determined by the measurements across the full diameter along <110> direction on the wafers.

3.3.2 SEM-EBIC Diffusion Length Measurements

Hole and electron diffusion lengths for n- and p-type LEC GaAs crystals were determined by the SEM-EBIC technique.[4-6] In this technique, the electron beam of a scanning electron microscope (SEM) is used to generate minority carriers which are collected by a Schottky diode. The Schottky diodes were fabricated by evaporating TiAu layers on both n- and p-type samples. The samples were cleaved through diodes. The measurements were made by scanning the electron beam (20 keV) along the cleaved face underneath a diode. The electron beam induced current (EBIC) was recorded as a function of distance from the Schottky barrier, as shown in Fig. 4 (a semi-log plot). The hole (or electron) diffusion length was determined from the inverse of the slope of the plot, i.e., $(d\ln I/dX)^{-1}$ in Fig. 4.

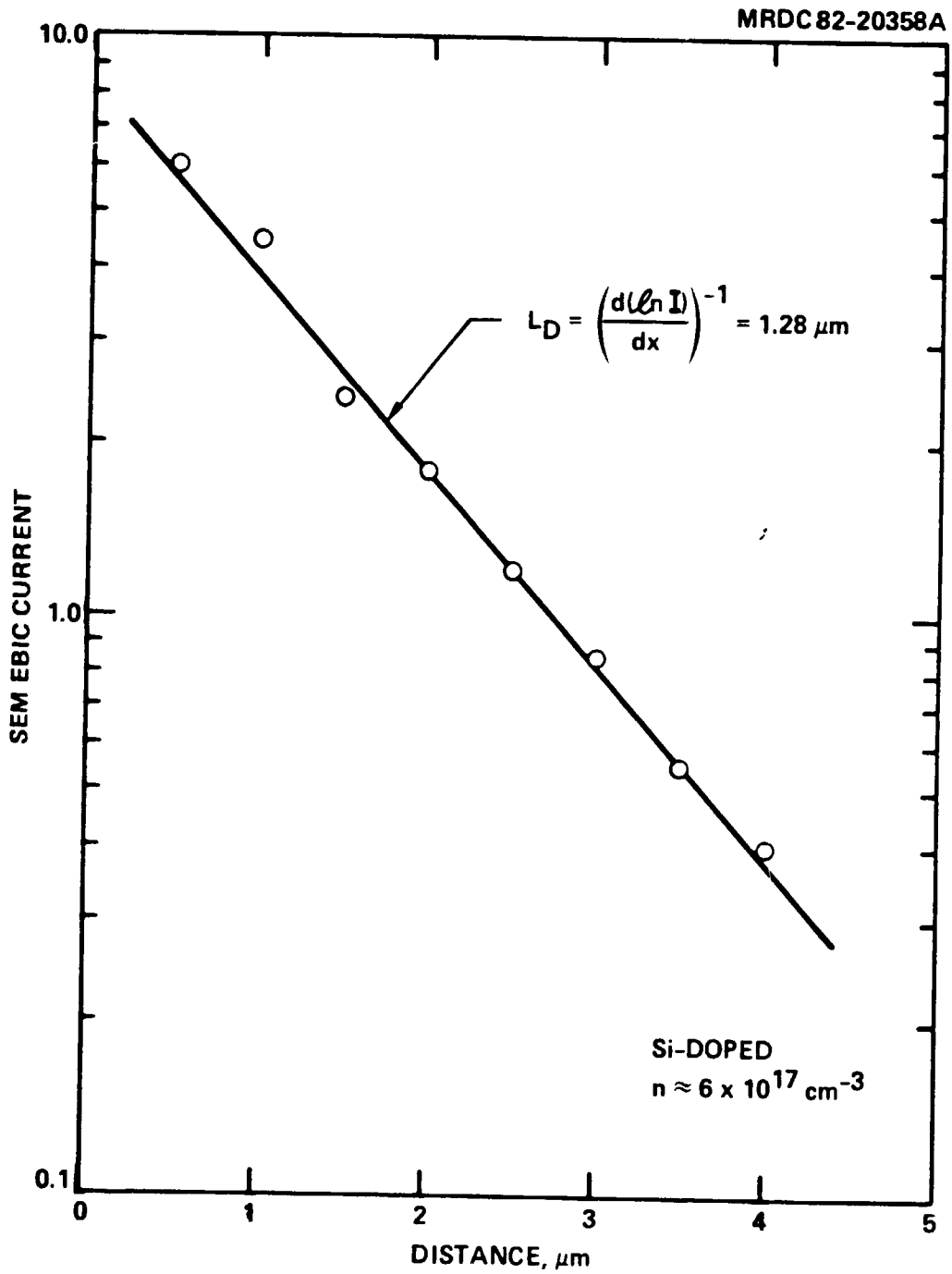

Fig. 4 SEM-EBIC measurement of minority carrier diffusion length. The log of the electron beam induced current is plotted as a function of distance from the Schottky diode. The diffusion length is obtained from the inverse of the slope of the curve.

4.0 RESULTS AND DISCUSSION

The results of crystallographic, impurity and electrical studies undertaken on n- and p-type LEC GaAs are described in this section.

4.1 Lattice Defect Studies

In this subsection, the lattice defects observed in n- and p-type LEC GaAs crystals will be presented in terms of dislocations, microstructures, dopant striations, and peripheral Ga-inclusions, respectively. The growth parameters responsible for dislocation density reduction as well as the mechanisms responsible for the dopant striations and peripheral Ga-inclusions will be discussed.

4.1.1 Dislocations

The results of dislocation studies of the front and tail of the NASA ingots are summarized in Table 3. In general, the measured EPD distributions across the full diameter of wafers follow a "W-shaped" profile. The average EPD increases from front to tail. These results are consistent with those observed in undoped LEC GaAs.[7] Note that the average EPD from the center and ring regions is essentially indicative of the entire wafer as these two regions account for over 75% of the area of the wafer.

As shown in Table 3, significant reductions in dislocation density were achieved at the front of two Se-doped ingots (R45 and R46) ([Se] > 1×10^{17} cm^{-3}) as compared to the EPD results of one of our typical undoped LEC GaAs ingots (R38) using similar growth parameters. In general, the higher Se-doping results in greater dislocation reduction. An EPD value as low as 5000 cm^{-2} achieved in the large annular area of the front wafer of the ingot (R46) with [Se] = 3×10^{18} cm^{-3}. Some reduction in dislocation density was also observed at the tail of these Se-doped ingots.

It is known that a principal cause of dislocations in bulk GaAs crystals is stress induced by thermal gradients during crystal growth. The use of

Table 3

Summary of Dislocation Studies of n- and p-Type Crystals Grown Under a Variety of Conditions

Sample No.		Crucible	Dopant	Carrier Density (cm^{-3})	EPD (cm^{-2})*** (1) Ring	(2) Center	(3) Edge
R38	F*	PBN	None	Semi Insulating	1.1×10^4	2.0×10^4	1.1×10^5
	T*				1.5×10^5	2.5×10^5	1.7×10^5
R43	F	Quartz	Si	7.5×10^{17}	1.5×10^4	4.4×10^4	9.1×10^4
	T			1.8×10^{18}	5.2×10^4	1.5×10^5	2.0×10^5
R45	F	Quartz	Se	6.0×10^{16}	9.0×10^3	3.0×10^4	9.8×10^4
	T			1.0×10^{17}	9.0×10^4	1.4×10^5	1.1×10^5
R46	F**	Quartz	Se	2.9×10^{18}	5.0×10^3	1.1×10^4	9.4×10^4
	T**			8.9×10^{18}	6.1×10^4	1.2×10^5	1.7×10^5
R47	F†	Quartz	Se	2.6×10^{18}	1.4×10^4	6.5×10^4	2.0×10^5
	T†			3.3×10^{18}	1.6×10^4	7.4×10^4	1.2×10^5
R50	F	Quartz	Zn	3.9×10^{17}	1.3×10^4	4.3×10^4	6.0×10^4
	T††			5.9×10^{17}	3.3×10^4	3.5×10^4	1.1×10^5

* Grown under NASA Contract NAS3-22224
** Grown under Rockwell IR&D
*** Each number represents an average of at least two measurements
† Thick B_2O_3 layer (~ 35 mm) used
†† Slow pull-free process

a thick B_2O_3 layer in LEC growth reportedly reduced the thermal gradient at the growth interface,[8] favoring further dislocation reductions in the ingot. However, no further reduction of the dislocation density (see Table 3) was achieved in one of the Se-doped ingots (R47, [Se] ~ 3×10^{18} cm^{-3}) using a thick B_2O_3 layer (~ 35 mm thick as compared to regular 17 mm), although a dislocation density of less than 5000 cm^{-2} was observed at several locations (<110> ring areas) in the front of the ingot. Our expectations of lowered dislocation densities were not met because of severe diameter fluctuations encountered using thick B_2O_3 as a result of the shallow radial temperature gradients. Diameter fluctuations increased the EPD and compensated the effect of the thick B_2O_3 layer. Finally, it is important to note that essentially no increase in EPD values was observed from the front to tail of this ingot, indicating some effects from the thick B_2O_3 layer.

It has been reported[9] that "dislocation-free" GaAs crystals can be grown by the Bridgman technique by doping with Si above the 2×10^{18} cm^{-3} level. However, no significant reduction of the dislocation density was observed in Si-doped crystals at impurity levels up to 2×10^{18} cm^{-3}. Our result can be explained by the fact that the viscosity of the B_2O_3 encapsulant decreased as a result of the dissolution of the elemental Si during the heatup cycle.[10] A decrease of viscosity increased the convective heat transfer from the crystal to the encapsulant, increasing the radial gradient and the dislocation density. We believe that the use of presynthesized, pre-Si-doped GaAs in the LEC puller would prevent pickup of Si by the B_2O_3 and enable significant reduction of the dislocation density.

Finally, no reduction of the dislocation density was observed in Zn-doped crystals with impurity levels up to 1×10^{19} cm^{-3}. However, a substantial reduction in the dislocation density was achieved at the tail of low Zn-doped crystal R50 (~ 3.5×10^4 cm^{-2}) by the use of a slow pull-free process, as shown in Table 3. In contrast to the normal pull-free process used to terminate growth, which involved the rapid pulling of the crystal from the melt, the improved process involves a gradual reduction of the diameter,

followed by lowering of the crucible. The new process essentially reduces the thermal shock experienced by the crystal during termination.

4.1.2 TEM Microstructures

In general, TEM microstructures were free of stacking faults, low-angle grain boundaries and dislocation loops in all of the undoped LEC GaAs ingots. The Si-($n \sim 2 \times 10^{18}$ cm^{-3}) and Zn-($p \sim 1 \times 10^{19}$ cm^{-3}) doped crystals were free of distinguishing features such as stacking faults as well. However, stacking faults and dislocation loops were observed in Se-doped material at impurity levels above about 1×10^{18} cm^{-3}, as shown in Fig. 5. Our results, summarized in Table 4, are consistent with work reported for high quality Bridgman material.

Table 4

Summary of TEM Studies of n- and p-Type Crystals

Sample No.	Dopant	Carrier Concentration (cm^{-3})	Stacking Fault (or Dislocation Loop)	
			Density (cm^{-3})	Size
R38F*	None	$\sim 10^7$ (Semi-Insulating)	0	-
R43T	Si	1.8×10^{18}	0	-
R45T	Se	1.0×10^{17}	0	-
R44F†	Se	1.0×10^{18}	$\sim 5 \times 10^{10}$	2000 A
R46T†	Se	9.0×10^{18}	$\sim 2 \times 10^{12}$	7000 A ~ 1.2 μm
R48F	Zn	8.0×10^{18}	0	-

*Grown under NASA contract NAS3-22224
†Grown under Rockwell IR&D

MRDC82-19988

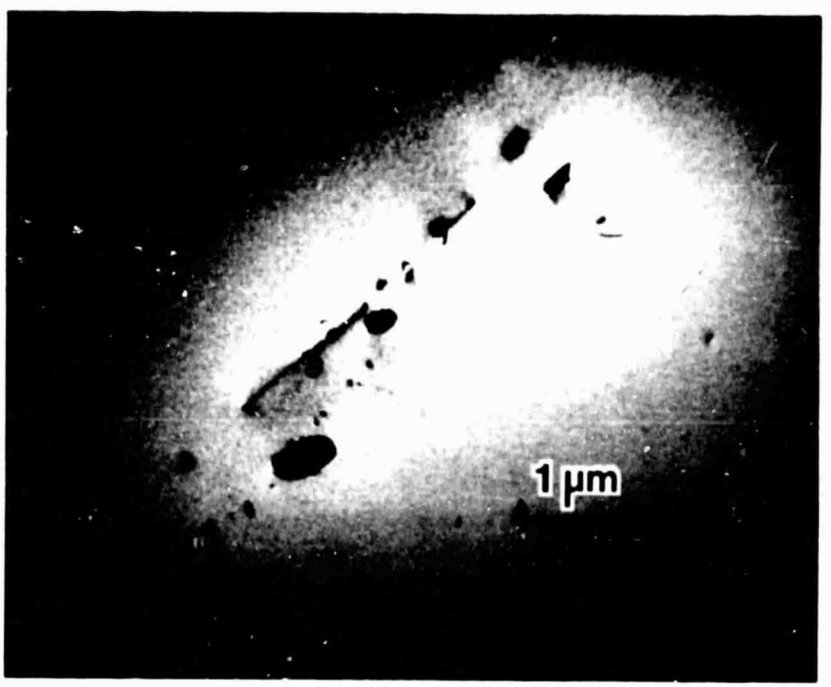

Fig. 5 Bright field TEM micrograph of Se-doped GaAs ($\sim 7 \times 10^{18}$ cm^{-3}) showing defects produced at high doping levels (see text).

4.1.3 Doping Striations and Peripheral Ga-Inclusions

Compositional inhomogeneities, or striations, are a well-known feature of crystals grown by the Czochralski technique. These inhomogeneities arise due to fluctuations in the microscopic growth rate or the thickness of the diffusion boundary layer. Fluctuations of the growth rate and boundary layer thickness can result from a variety of causes, including convection in the melt, crystal rotation in a thermally asymmetric environment, and mechanical vibrations in the crystal pulling mechanism. Despite some of the potentially adverse effects of striations in crystals on the electrical properties of the material, they can be a useful means for studying the crystal growth process.

We have used infrared (IR) microscopy to reveal striations in our Si, Se, and Zn doped crystals. The pattern of the striations was used to evaluate the interface shape in the cone region of the crystals (the striations are essentially parallel to the growth interface).

Figure 6 depicts the change in interface shape during the growth of the cone of a crystal as determined by IR studies of the dopant striations. Micrographs of striations in selection regions are also shown. Several important features can be seen in this figure. First, since the interface is isothermal, the interface shape shows the direction of heat flow during growth because heat flows perpendicular to isotherms. The interface near the seed is nearly flat, indicating heat flow by conduction up the seed. As the diameter of the crystal increases, the interface becomes convex with respect to the solid. About halfway through the growth of the cone, some concave curvature develops near the edge of the crystal, indicating that some heat is actually flowing out to the B_2O_3. By the time the crystal reaches full diameter, the curvature of the interface is convex in the central region and concave near the edges. The curvature at this point is pronounced. This tells us that when the crystal reaches full diameter and the length of the crystal exceeds the thickness of the B_2O_3, the heat flow at the interface is predominantly due to conduction up the crystal, with some convective heat loss to the B_2O_3.

MRDC82-20368

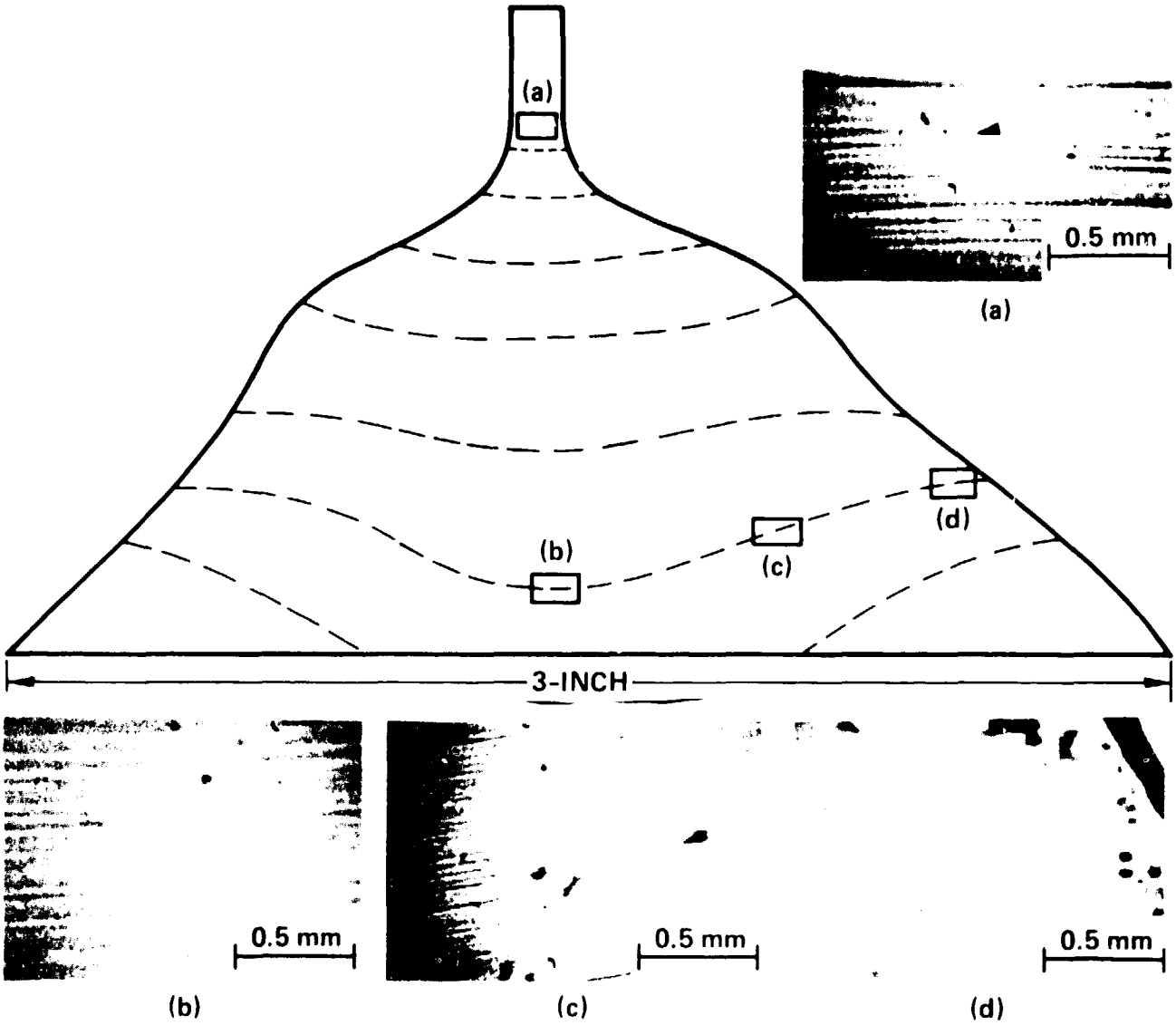

Fig. 6 Infrared micrograph showing dopant striations and interface shape in cone of n-type ingot. The striations are "rotational" and are probably caused by fluctuations in microscopic growth rate. The interface shape, determined from the morphology of the striations across the crystal, becomes progressively more convex in the central region of the crystal and more concave near the edges.

The morphology of the striations also tells us something about the growth conditions. The striations are predominantly parallel to each other. Also, the measured interstriation spacing (2.4×10^{-2} mm) is in agreement with the calculated value, assuming one striation is produced per rotation of the crystal. Therefore, it can be concluded that the striations are of the so-called "rotational" class (as opposed to nonrotational), indicating that they are due to variations of the microscopic growth rate across the interface as the crystal rotates in a thermally asymmetric environment.

Finally, two other observations are of interest. First, the curved white lines seen in the background of Fig. 6a are believed to be dislocation lines, and we are currently investigating these structures in more detail. Second, we have found that IR microscopy can reveal Ga inclusions, shown in Fig. 7, that form at the periphery of the crystal during post-growth cooling. The vertical "tracks" above each inclusion apparently mark the trail of the Ga as it thermally migrated into the crystal.

4.2 Impurity Characterization

The results of impurity characterization, including background impurities, and longitudinal and radial dopant distribution in the doped LEC crystals will be presented in this subsection. The effective segregation coefficients for Si, Se and Zn will be determined, and the possible mechanism responsible for "W"-shaped radial dopant distribution will be discussed.

4.2.1 Background Impurities

The SIMS analysis of the n- and p-type LEC GaAs crystals is summarized in Table 5. The typical total concentration of background donors and acceptors is about 1×10^{16} cm^{-3}. The background impurity concentration is comparable to that of high-purity, undoped LEC GaAs crystals, as well as undoped Bridgman-grown GaAs crystals, as indicated in Table 6. It is of interest to note that boron in Si-doped LEC GaAs crystals can be two to three orders of magnitude higher (increasing from typically low 10^{16} (undoped) to

MRDC82-20366

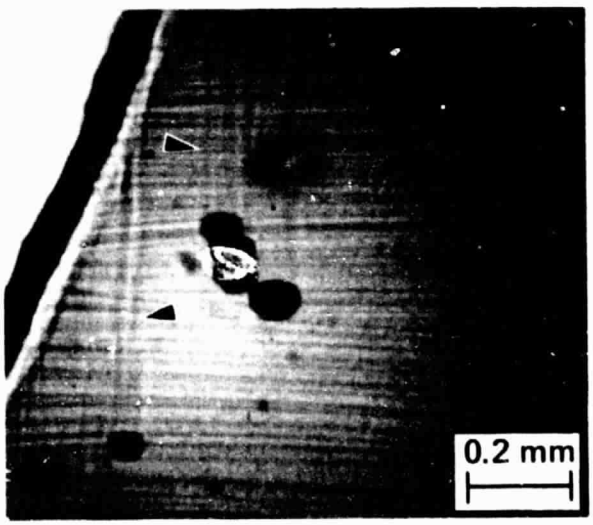

Fig. 7 Infrared micrograph taken at the edge of a doped crystal in the cone showing inclusions and "tracks" of the inclusions left as they migrated into the crystal from the surface.

low 10^{19} cm^{-3} (R43)) than in Bridgman material, as shown in Table 6. Si dissolution in B_2O_3 could be responsible for this behavior. However, B is an isoelectronic impurity in GaAs, and no indication of the electrical activity of B in GaAs has been observed.

Table 5

SIMS Analysis of Chemical Impurities in Doped LEC GaAs

Sample No.		Crucible	Dopant	Impurity Concentration (cm^{-3})								
				Si	Se	Te	S	Mg	Cr	Mn	Fe	B
R43	F	Quartz	Si	1e18	<e14	<e14	4e14	4e14	4e14	2e15	4e15	2e19
	T		Si	3e18	<e14	<e14	1e15	8e14	5e14	2e15	7e15	6e19
R45	F	Quartz	Se	5e15	2e16	<e14	3e14	<e14	3e14	4e14	2e15	2e16
	T		Se	9e15	7e16	<e14	5e14	<e14	2e14	3e14	2e15	6e16
R47	F	Quartz	Se	7e15	1e19	<e14	5e15	1e14	3e14	1e15	1e15	8e16
	T		Se	1e16	1e19	<e14	6e15	1e14	2e14	6e14	1e15	1e17
R50	F	Quartz	Zn	2e16	<e14	6e14	2e15	1e14	3e14	3e14	2e15	3e16
	T		Zn	1e16	<e14	<e14	6e14	<e14	3e14	3e14	2e15	6e16

Table 6

Comparison of Background Impurity Levels in LEC and Bridgman GaAs

Growth Technique	Dopant	Crucible	S	Se	Te	Mg	Cr	Mr	Fe	C*	Si	B
LEC[a]	Se or Si or Zn	Quartz	2e15	<1e14	<1e14	2e14	<5e14	<1e15	<3e15	NM[d]	2e15-2e16	8e15-4e19
LEC[b]	None	Quartz	1.3e15	<1e14	<1e14	<5e14	<5e14	<1e15	<3e15	~ 3e15 (ND-9e15)	5e14-3e16	4e14-2e17
Bridgman[c]	None	Quartz	3e15	3e14	4e13	5e14	<5e14	5e14	5e15	ND[e]	2e16	<2e14

* Carbon determined by LVM

[a] 8 crystals analyzed and averaged

[b] 7 crystals analyzed and averaged

[c] 4 crystals analyzed and averaged

[d] not measured

[e] not detectable

4.2.2 Dopant Distribution

Longitudinal (along the crystal growth axis) and radial dopant densities were determined from profiles of the free carrier concentration across the top (cone), front, middle and tail wafers of LEC ingots. As described in Section 3.3.1, room temperature Hall effect measurements were used to measure free carrier concentration.

4.2.2.1 Longitudinal Dopant Distribution and Effective Segregation Coefficient

The longitudinal distribution of the free electron and hole concentration in n- and p-type 3 inch LEC GaAs ingots are summarized in Tables 7 and 8, respectively. As shown in these tables, free carrier concentrations (e.g., dopant concentrations) always increase from the (cone) top to tail of ingots regardless of the dopant. Chemical analysis of the longitudinal distributions of Si and Se by SIMS (Table 5) agree with the electrical measurements.

It is known[11] that when a crystal is grown from a melt by progressive freezing from one end, e.g., by the Czochralski process, and the liquid phase contains a uniformly distributed impurity, then the incorporation of the impurity into the solid can be described by

$$C = C_0 k_0 (1 - g)^{k_0 - 1} \qquad (1)$$

where C is the impurity concentration in the solid, C_0 is the initial impurity concentration, k_0 is the equilibrium segregation coefficient, and g is the fraction of the melt solidified. Taking the logarithm of each side of Eq. (1) yields

$$\log C = \log C_0 k_0 + (k_0 - 1) \log (1 - g) \quad . \qquad (2)$$

A plot of log (free carrier concentration) vs log (1 - g) yields a straight line with a slope of $k_0 - 1$.

The segregation coefficients, k_0, for Si, Se or Zn along the NASA LEC GaAs crystals were determined by the above analysis using corresponding values of g and C (free electron or hole concentration) for each crystal (See Tables 7 and 8, and Fig. 8). Values of 0.19, 0.52 and 0.47 were determined for the segregation coefficients for Si, Se and Zn, respectively. For comparison, we also estimated the equilibrium segregation coefficient for the dopant from the melt to the crystal, k_0', by taking the ratio of the free carrier concentration at the cone-top to the added dopant concentration. As shown in Table 9, these estimated k_0' values are close to our calculated k_0 values except for the dopant Si, which shows a tremendously lower k_0' value. This effect is due to the severe Si-dopant loss to the B_2O_3 encapsulant as discussed in Section 4.1.1. Our experimental values of k_0 and k_0' are consistent with published data for both LEC[12] and non-LEC[13] GaAs crystals as shown in Table 9.

Table 7

Free Electron Profiles along n-Type LEC GaAs

Wafer No.	Dopant	Averaged Electron Density (cm^{-3})
R43 Cone Top	Si	6.2×10^{17}
Front	Si	8.0×10^{17}
Tail	Si	1.8×10^{18}
R45 Cone Top	Se	5.8×10^{16}
Front	Se	6.0×10^{16}
Middle	Se	7.6×10^{16}
Tail	Se	1.1×10^{17}
R47 Front	Se	2.6×10^{18}
Tail	Se	3.3×10^{18}

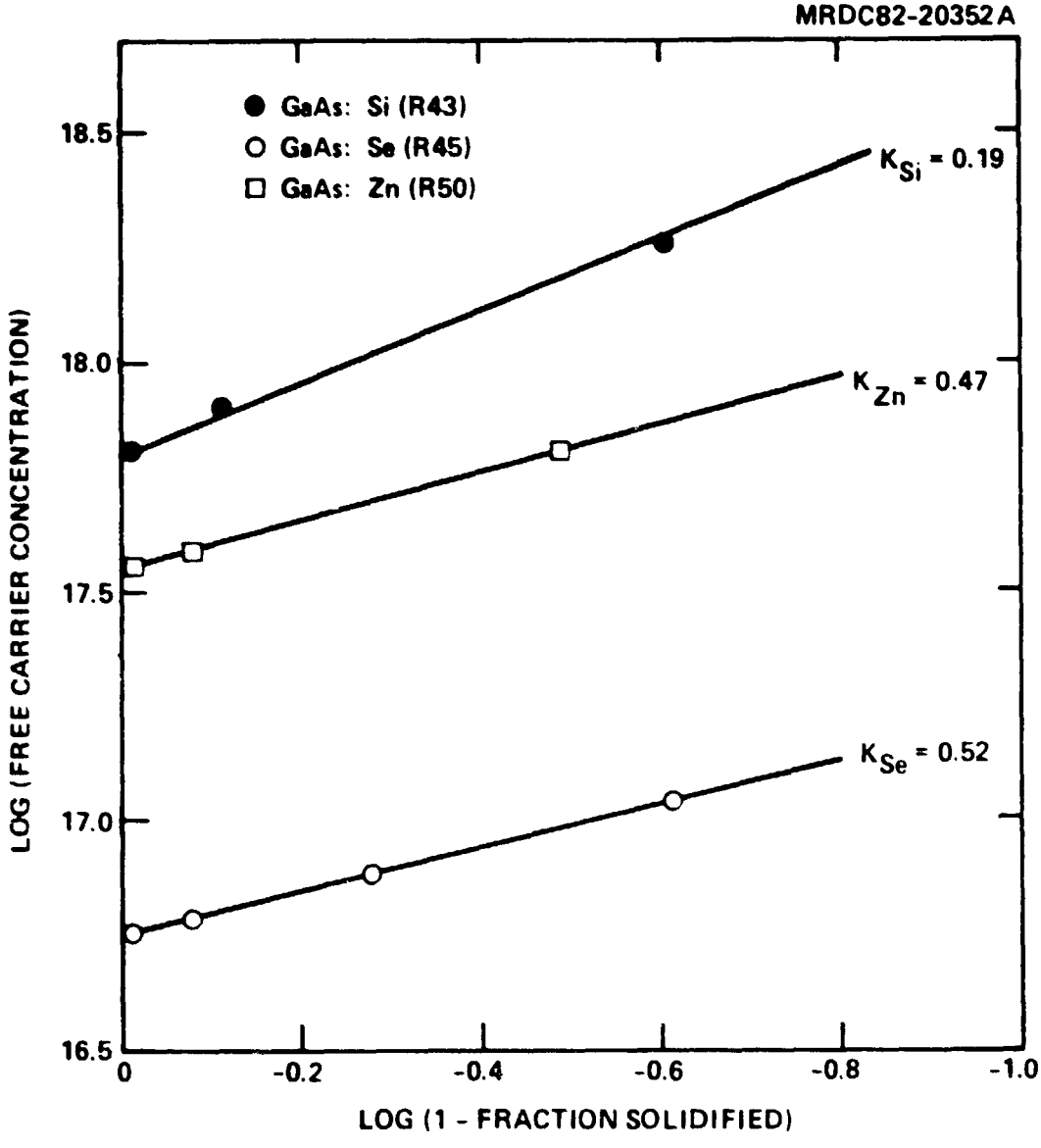

Fig. 8 Determination of equilibrium segregation coefficient by plotting log C as a function of log (1-g).

Table 8
Free Hole Density Along p-Type LEC GaAs

Wafer No.	Dopant	Averaged Hole Density (cm^{-3})
R48 Cone Top	Zn	6.2×10^{18}
R50 Cone Top	Zn	3.7×10^{17}
Front	Zn	3.9×10^{17}
Tail	Zn	6.4×10^{17}

4.2.2.2 Radial Dopant Distribution

Figure 9 shows the radial dopant profiles across 3 inch diameter wafers from the front and tail of Si- and Se-doped LEC ingots. The profiles are essentially "W"-shaped in these wafers. In general, the lower dopant variations (< ± 10%) were observed in the tail wafers as compared to those (~ ± 15%) of the front wafers. Similar "W"-shaped profiles were also observed in Zn-doped LEC ingots.

The origin of the "W"-shaped profiles could be associated with variations across the solidification front of the diffusion boundary layer thickness. The boundary layer thickness variations presumably are due to convective melt flows. The basic flow pattern in the melt in our crystal growth configuration, projected from the work of Carruthers and Nassau,[14] is divided into two separate non-mixing cells. One cell lies beneath the crystal, as shown in Fig. 10. Outside this cell, the liquid rotates as an almost solid body. Because we use isorotation, with crucible and crystal rotation rates of 15 and 6 rpm, respectively, the liquid within the central cell is expected to spiral vertically at the outside and fall in the center, as indicated in the figure. This flow pattern could give rise to local maxima in the boundary layer thickness near the center and edge of the crystal. Basic segregation

Table 9

Comparison of Values of the Equilibrium Segregation Coefficient Obtained on NASA Program and Previously Published Values

Ingot No.	Dopant	$[Dopant]_{Melt}$ (cm^{-3})	$[Free\ Carrier]_{Cone\ Top}$ (cm^{-3})	k_o*	k_o'†	Published k_o Values	
						LEC (Ref. 12)	Non-LEC (Ref. 13)
R43	Si	2.4×10^{19}	6.2×10^{17}	1.9×10^{-1}	2.6×10^{-2}	1.85×10^{-2}	1.4×10^{-1}
R45	Se	1.85×10^{17}	5.7×10^{16}	5.2×10^{-1}	3.1×10^{-1}	5.0×10^{-1}	3.0×10^{-1}
R50	Zn	1.03×10^{18}	3.7×10^{17}	4.7×10^{-1}	3.6×10^{-1}	N/A	4.0×10^{-1}

*k_o = Equilibrium segregation coefficient along ingot (see Fig. 8).

†k_o' = Equilibrium segragation coefficient from melt to ingot (see text).

N/A = Not available.

SCB2-10913

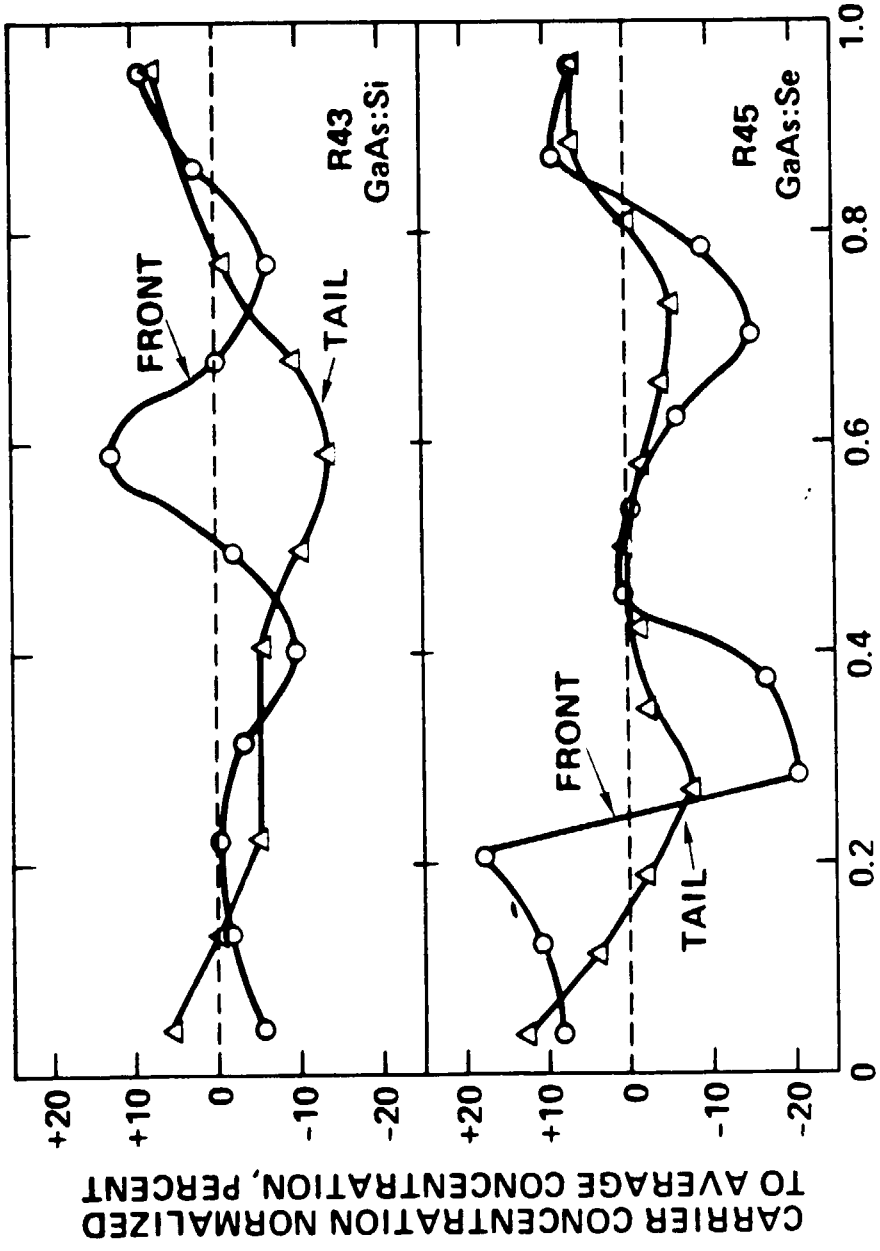

Fig. 9 Dopant profiles across 3-in. LEC wafers.

MRDC82-16930A

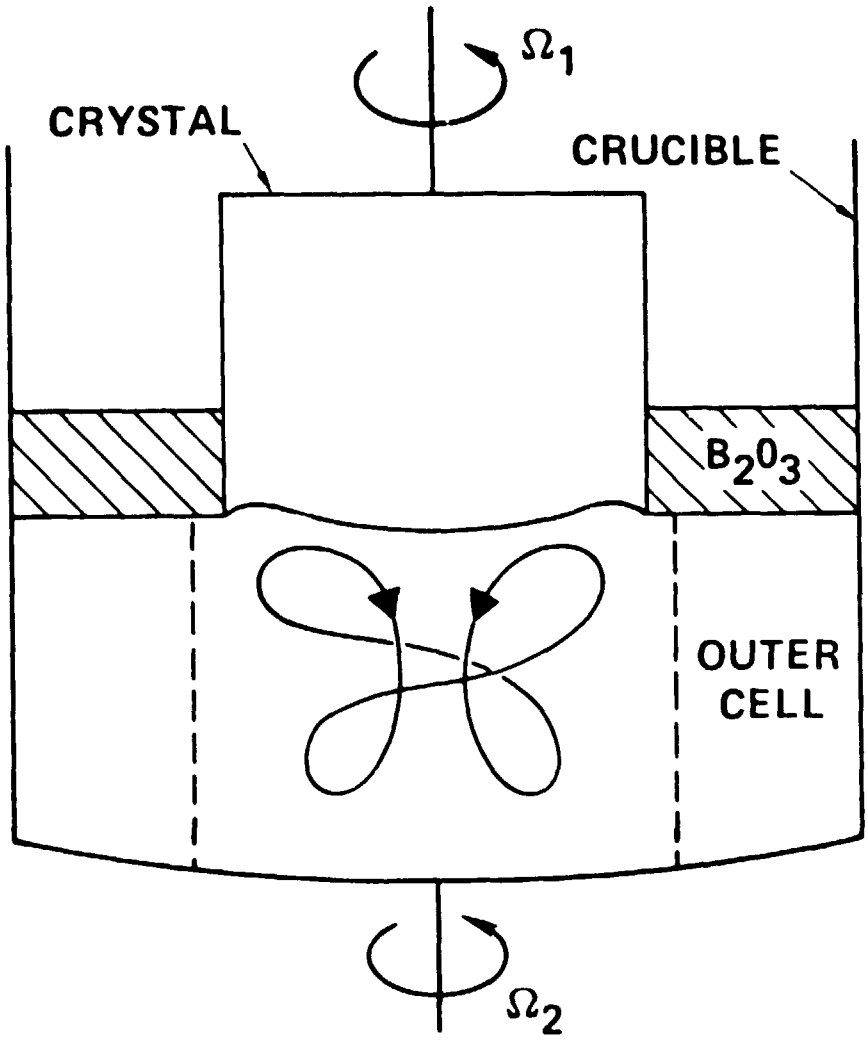

Fig. 10 Convective flow pattern in the melt that could lead to a "W"-shaped dopant profile across the crystal diameter.

theory shows[15] that the dopant concentration increases as the boundary layer thickness increases for impurities, such as Si, Se, and Zn in GaAs, which have distribution coefficients (k_0) less than 1. Therefore, the "W"-shaped dopant profiles were observed in Si-, Se- or Zn-doped LEC GaAs ingots. Further, the lower dopant variations observed in the tail wafers are probably due to the change of convection flow pattern induced by the lowering of melt height at the end of the crystal growth.

4.3 Electrical Properties

In this subsection, the results on the free carrier mobility and the minority carrier diffusion length will be presented. The effect of dislocation density and EL2 concentration on the diffusion length will be discussed.

4.3.1 Mobility

The dependence of the electron mobility on the free carrier concentration of LEC material is shown in Fig. 11. The Se-doped LEC samples have mobilities ranging from 4100 to 1700 $cm^2/V\text{-}s$ corresponding to electron densities of 6×10^{16} to 4×10^{18} cm^{-3}. A slightly lower moblity is observed for the Si-doped samples with similar electron densities indicating higher compensation. The mobilities for the samples with electron densities lower than $\sim 6 \times 10^{16}$ cm^{-3} are also shown in Fig. 11. These samples were grown from quartz crucibles without intentional doping (Si-contamination from the quartz crucible). As shown in Fig. 11, the mobility curves show a peak and a valley at an electron density of $\sim 8 \times 10^{16}$ and 2×10^{16} cm^{-3} respectively, indicating significantly higher compensation in samples with electron densities below $\sim 2 \times 10^{16}$ cm^{-3}. This higher compensation is probably due to background impurities or native defects in LEC GaAs ingots. Furthermore, our mobility results are consistent with statistical analysis of hundreds of crystals grown by conventional bulk-grown methods reported recently by Mullin et al.[12] In addition, a comparison of our results with the theoretical mobility-electron concentration relationship for GaAs indicates that our material is characterized by low

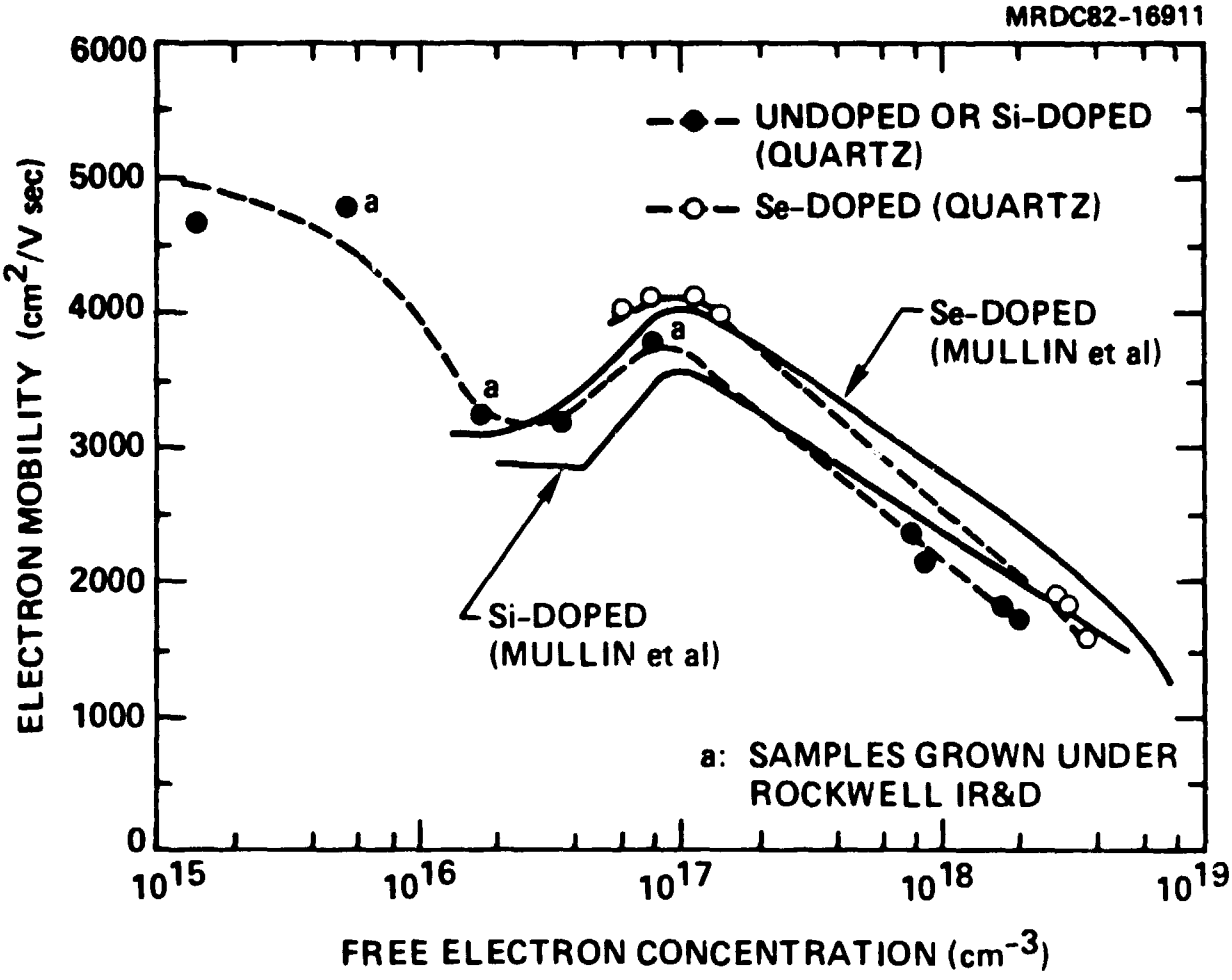

Fig. 11 Electron mobility as a function of electron concentration in n-type GaAs. Our results are very similar to a statistical analysis of samples reported by Mullin et al.[1.12]

compensation ratios (0.3 to 0.4) consistent with the statistical behavior of other bulk GaAs materials.[12]

Generally high hole mobilities were observed for the p-type LEC GaAs, as shown in Fig. 12. Hole mobilities as high as 320 $cm^2/V\text{-}s$ (for hole concentration ~ 1×10^{16} cm^{-3}) were observed for the LEC material grown from undoped Ga-rich melt using a PBN crucible. Mobilities as high as 210 $cm^2/V\text{-}s$ were observed for the Zn-doped material with ~ 4×10^{17} cm^{-3} hole concentration. Elliott et al.[16] at Rockwell MRDC have explained the p-type conduction of the undoped LEC GaAs in terms of the 77 meV acceptor. The origin of this acceptor is probably the Ga_{As} antisite defect. These results show that the mobility of the p-type LEC GaAs is comparable to commercial Bridgman-grown GaAs, as shown in Fig. 12.

4.3.2 Minority Carrier Diffusion Length

Good hole diffusion lengths (as high as 1.4 μm) were measured in n-type (Se- or Si-doped) LEC GaAs crystals, as shown in Fig. 13. The measured values are comparable to those of n-type bulk GaAs grown by conventional methods reported by Sekela et al.[17] As shown in Fig. 14, the electron diffusion length was also determined for p-type LEC GaAs crystals. For samples grown from Ga-rich melt in a PBN crucible (hole densities ~ 1×10^{16} cm^{-3}), a diffusion length as long as 5.3 μm was observed. This value is exceptionally high for bulk GaAs, and actually compares favorably with diffusion lengths (~ 8 μm) reported for p-type, high-purity MOCVD and LPE layers.[5,6,18] However, much lower electron diffusion lengths (0.37 to 0.70 μm) were observed for Zn-doped LEC crystals which had hole densities from 4×10^{17} to 8×10^{18} cm^{-3}.

4.3.3 Effect of Dislocation Density and EL2 Concentration on Diffusion Lengths

Dislocations in GaAs can act as minority carrier recombination centers, adversely effecting the performance of minority carrier devices, such as solar cells. Figures 15 and 16 show plots of the minority carrier diffusion

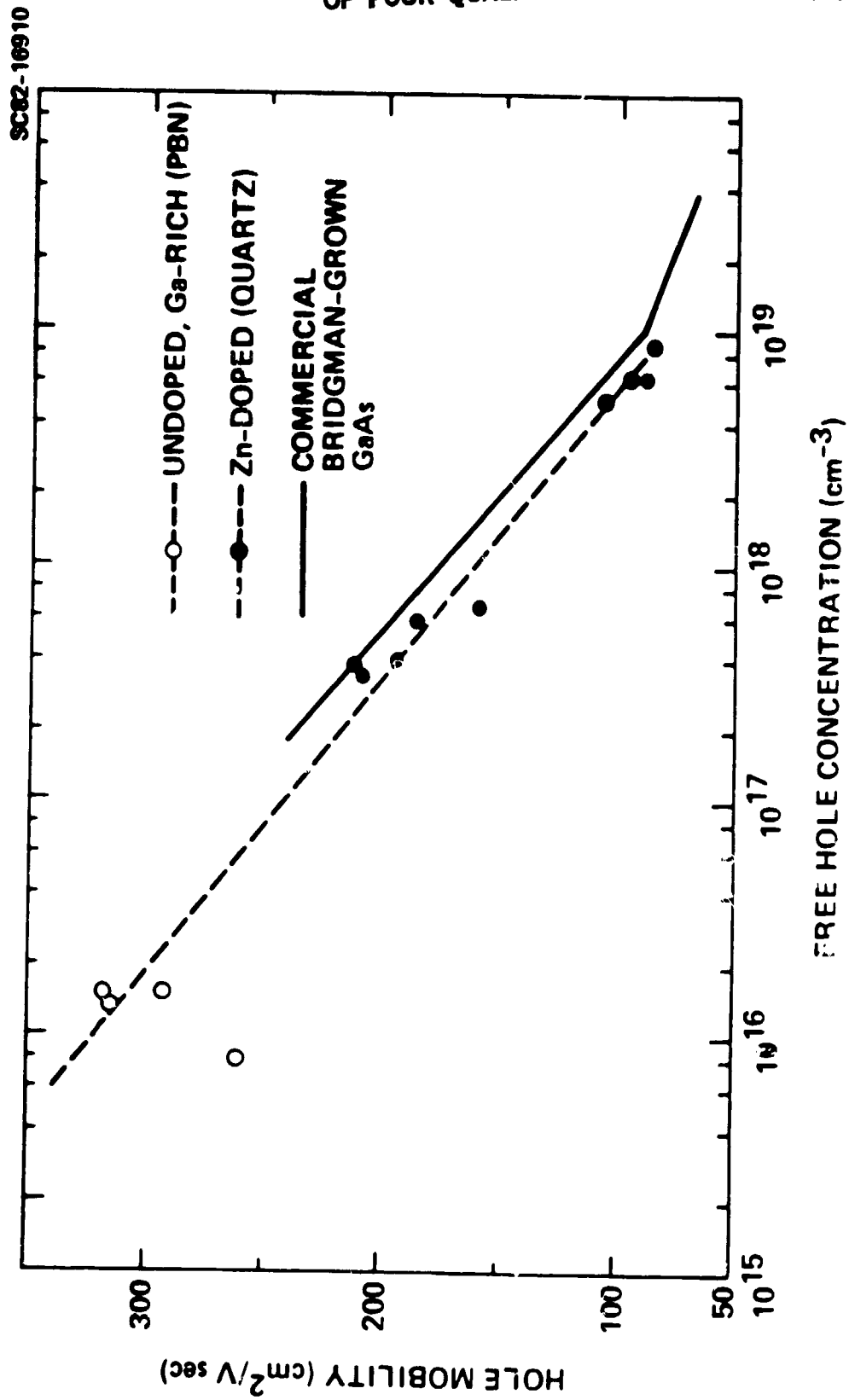

Fig. 12 Hole mobility as a function of hole concentration in Zn-doped and undoped p-type GaAs. The parameters of the LEC material are comparable to Bridgman material.

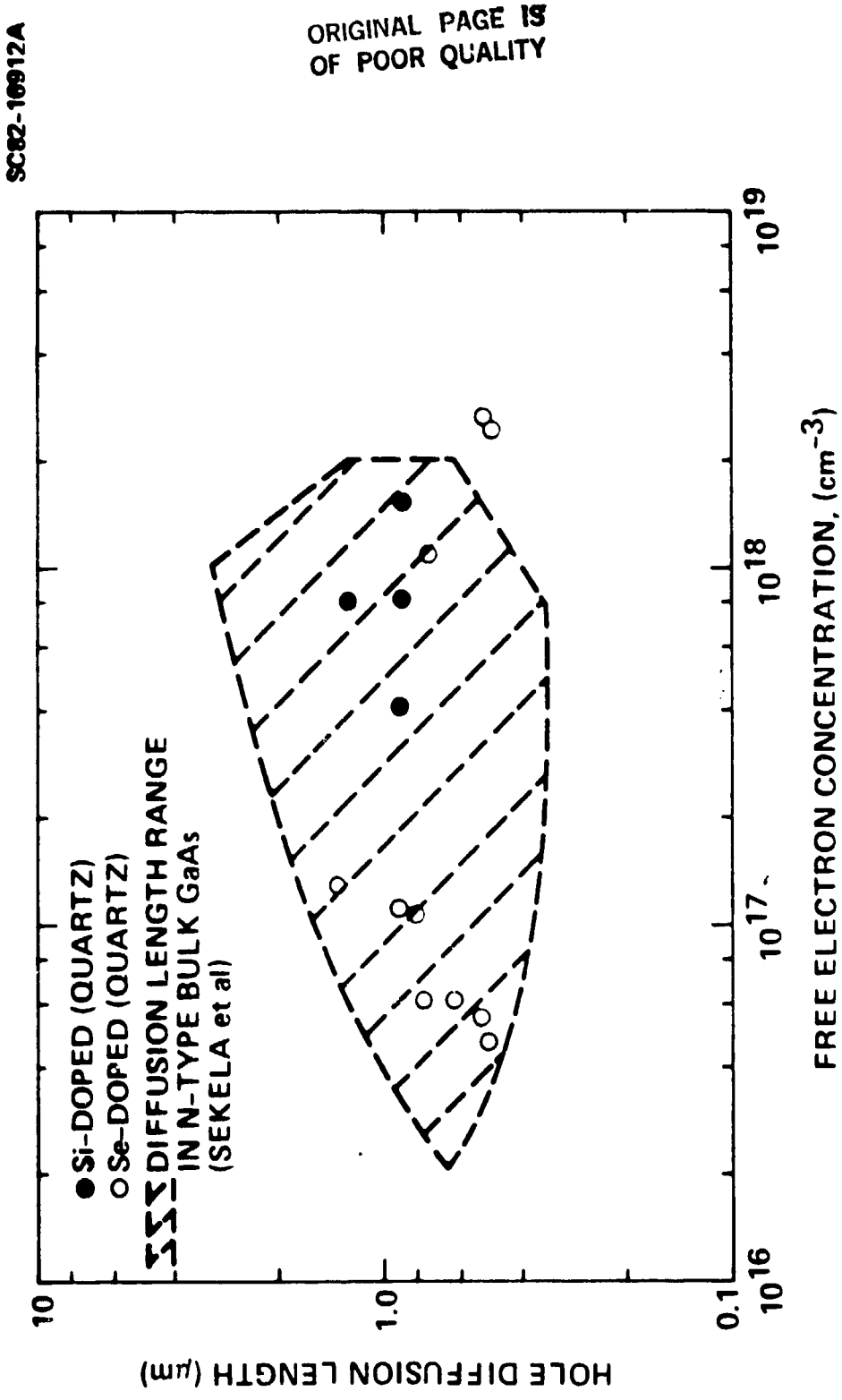

Fig. 13 Minority carrier diffusion length in n-type material as a function of the electron concentration.

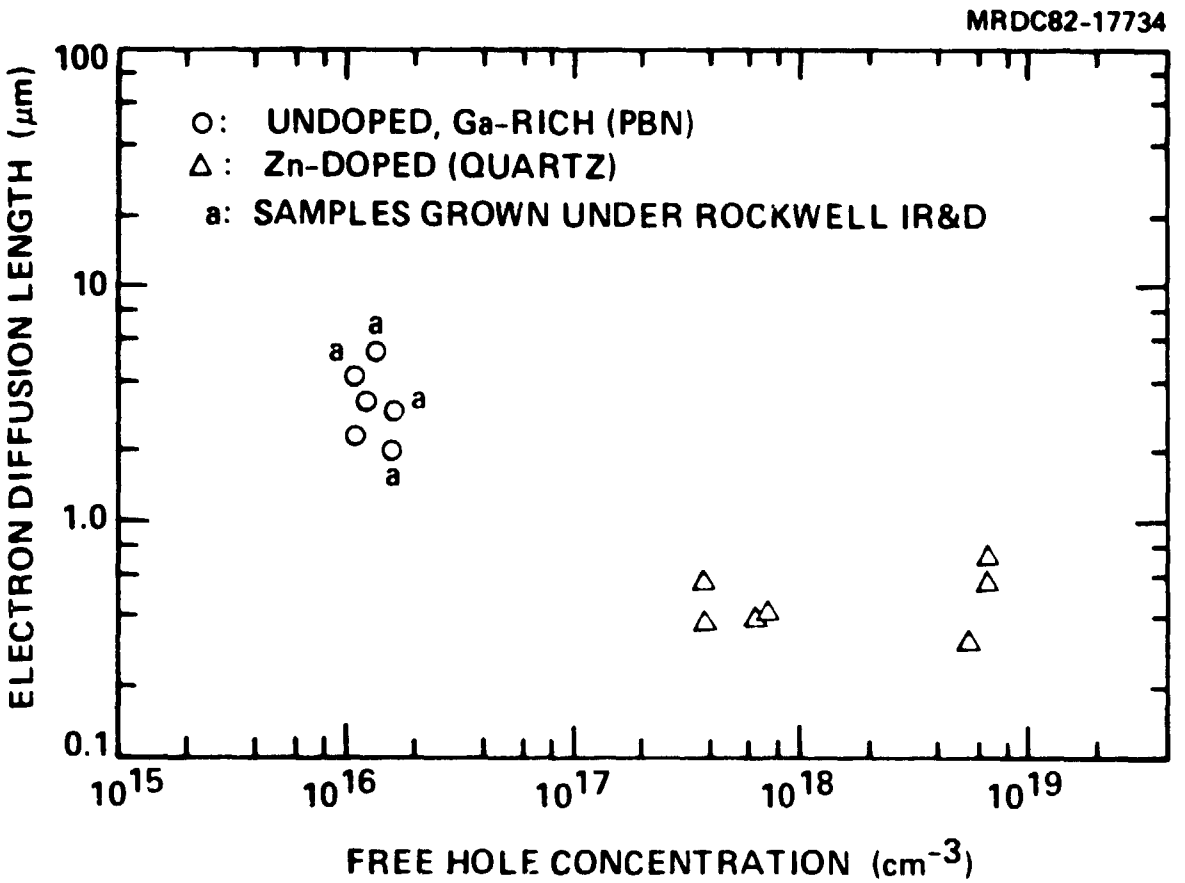

Fig. 14 Minority carrier diffusion length in p-type material as a function of the hole concentration.

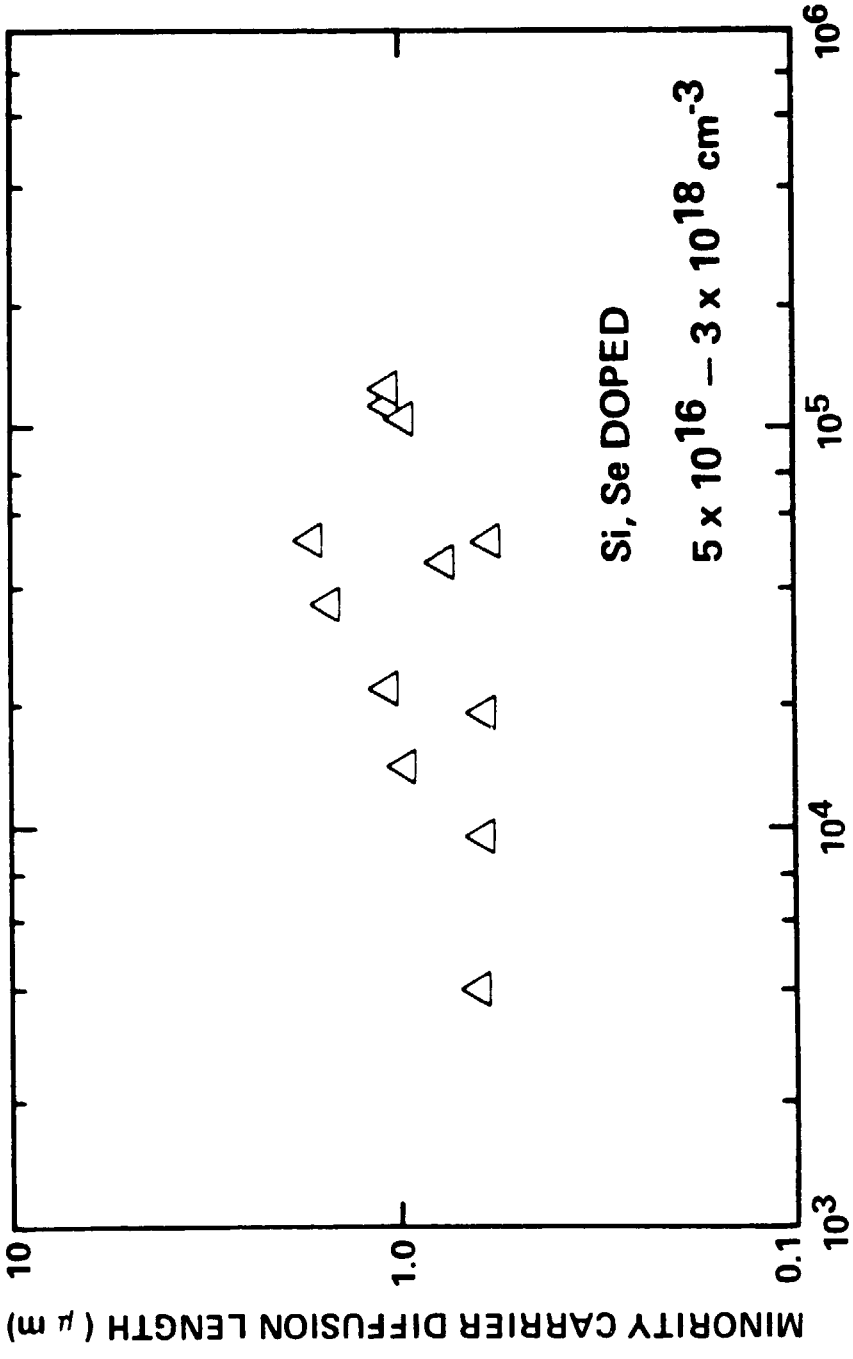

Fig. 15 Minority carrier diffusion length in n-type material as a function of the dislocation (etch pit) density. The diffusion length is independent of the dislocation density over the range indicated.

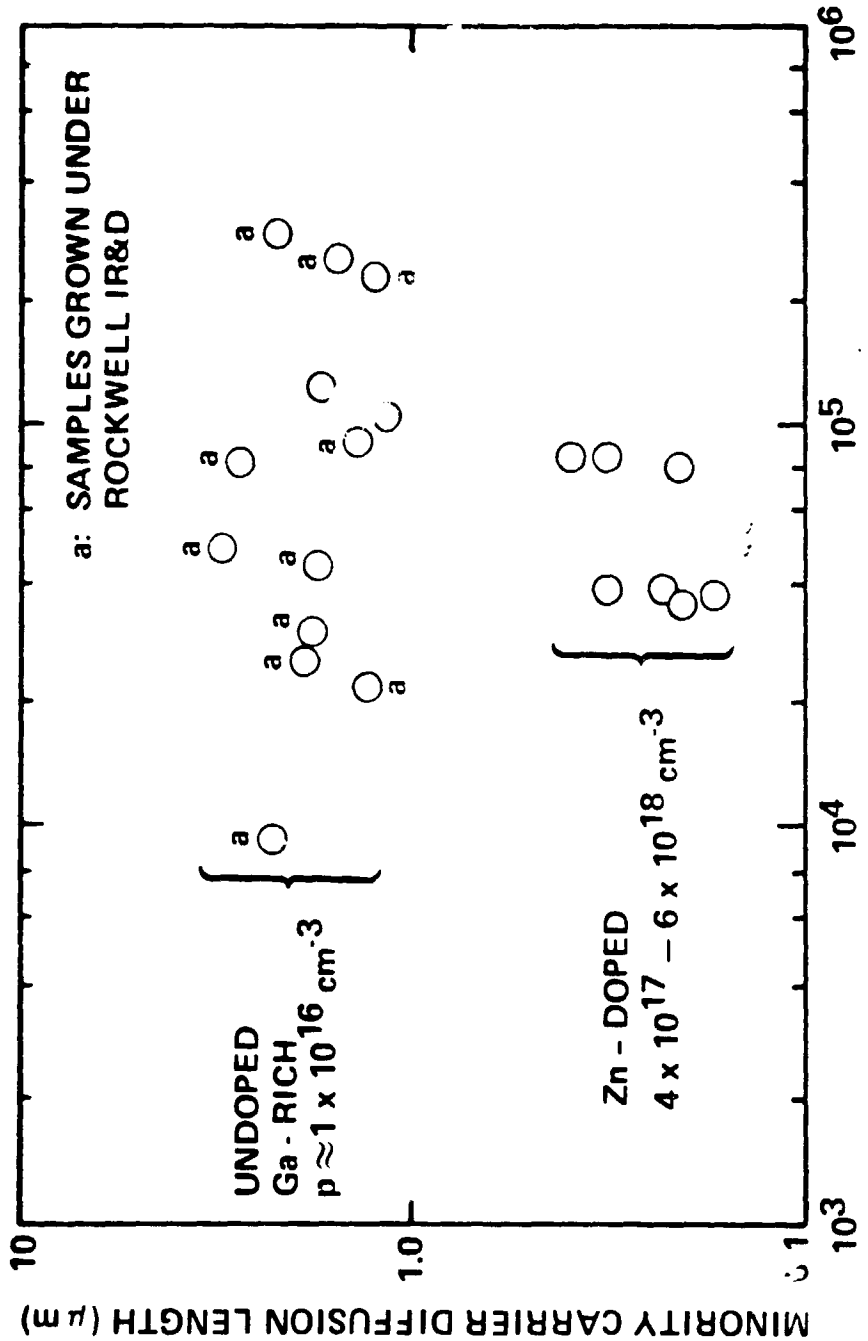

Fig. 16 Minority carrier diffusion length in p-type material as a function of the etch pit density. The diffusion length is independent of the dislocation density over the range indicated. The relatively short diffusion length in the Zn-doped material could be done in part to the high concentration of EL2, which behaves as an electron trap (see Fig. 17).

length versus the dislocation density for n- and p-type LEC GaAs, respectively. Both hole and electron diffusion lengths do not depend on dislocation density for densities ranging from 5×10^3 to 5×10^5 cm^{-2} observed in these materials. This conclusion is consistent with the argument that the distance between dislocations (e.g., 15 ~ 150 μm for 5×10^3 ~ 5×10^5 cm^{-2} EPD) is much longer than the diffusion length (e.g., 0.4 ~ 5.3 μm).

As shown in Fig. 14, the diffusion length in Zn-doped crystals is approximately a factor 5 lower than in undoped, Ga-rich LEC crystals. It has been reported that the electron diffusion length is relatively constant for both p-type LPE[18] and bulk[19] GaAs with carrier concentrations below 1×10^{18} cm^{-3}. Therefore, the substantial difference between the Zn-doped and the undoped material can probably not be completely accounted for in terms of the difference in hole concentration. The results shown in Fig. 14 indicate that some minority carrier trapping centers are possibly responsible for the reduction of diffusion length observed in Zn-doped LEC material. Figure 17 shows a plot of electron diffusion length as a function of arsenic atom fraction in the melt corresponding to the growth conditions of the Ga-rich and Zn-doped LEC material. We have reported[2,3] that formation of deep donor trapping center EL2 is controlled by the melt stoichiometry. The EL2 concentration increases as the As atom fraction in melt increases as indicated in Fig. 17. Since these Zn-doped crystals were grown under near stoichiometric conditions, higher EL2 concentrations were present in these crystals, probably accounting for the lower diffusion lengths.

Finally, our results indicate that bulk n- or p-type material intentionally doped to any level would have the highest electron diffusion length when grown under Ga-rich conditions. Furthermore, work should be pursued in this area.

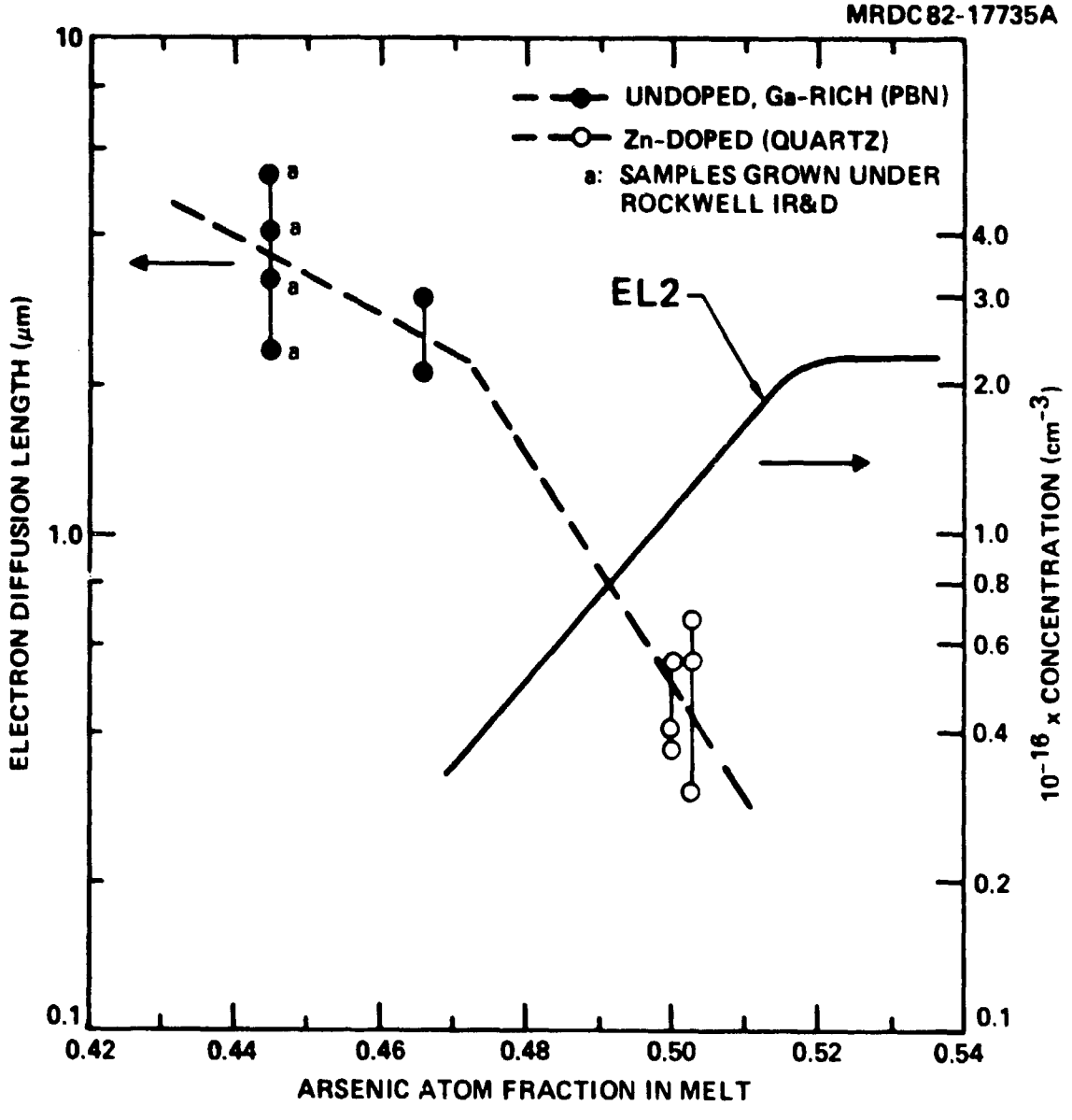

Fig. 17 Comparison between the dependence of the electron diffusion length in p-type material and the EL2 concentration on the melt stoichiometry. The decreasing diffusion length corresponds to an increasing EL2 concentration, indicating the role of EL2 as an electron trap in the Zn-doped material.

5.0 SUMMARY

Important milestones have been achieved on the NASA "Growth and Characterization of Czochralski-Grown n- and p-type GaAs for Space Solar Cell Substrates" at MRDC. First, it has been shown that the average dislocation density throughout the entire central region (defined by about 80% of the diameter) of 3-in. wafers can be controlled to a value below 1×10^4 cm^{-2}. The dislocation density in selected regions can be as low as 5000 cm^{-2}. This result is achieved by using Se-doping and optimal growth parameters for dislocation density reduction developed in this program and investigated for previously undoped LEC crystals. These results represent a substantial improvement over commercial 2-in. diameter LEC material, which typically has a dislocation density higher than 5×10^4 cm^{-2}. Our results also show that the slow pull-free process and the use of thick B_2O_3 encapsulant layer are effective in reducing the dislocation multiplication towards the tail of the crystal.

Second, it was shown that the concentration of background impurities in the doped LEC material can be reduced to the level of 7×10^{15} cm^{-3} through proper control of the material synthesis, growth and doping conditions. This purity is consistent with that of undoped LEC GaAs reported in the previous NASA final report, indicating the doping technique used in the program did not induce additional electrical-active centers in the crystals. The studies of radial dopant distributions also showed good dopant uniformity was achieved in our LEC crystals. Dopant variations are typically within $\pm$ 15% of the average concentration across 3-in. wafers. These results are comparable, if not superior to that of commercial Bridgman material.

Third, our experimental results have also shown that excellent electrical properties are achieved in these doped LEC crystals. Good electron mobilities ranging from 4200 to 1700 $cm^2/V\text{-}s$ corresponding to electron densities of 6×10^{16} to 4×10^{18} cm^{-3}, were observed in n-type (Si- or Se-doped) LEC crystals. This also indicated low compensation ratios (0.3 to 0.4)

in these crystals. Hole mobilities as high as 320 $cm^2/V\text{-}s$ (for a hole concentration ~ 1×10^{16} cm^{-3}) and 210 $cm^2/V\text{-}s$ (for a hole concentration ~ 4×10^{17} cm^{-3}) were observed for the p-type LEC material grown from an undoped Ga-rich melt and a Zn-doped melt, respectively. These results are comparable to commercial, high-quality Bridgman-grown GaAs, and are also consistent with our observation of the low background impurity concentration. Furthermore, good electron diffusion lengths (as high as 5.4 μm) as well as hole diffusion lengths (as high as 1.4 μm) were obtained in n-type and p-type LEC GaAs crystals. No effect of the dislocation density was observed on the diffusion lengths. This result is consistent with the combination of low dislocation densities with long diffusion lengths which represent much longer distances between dislocations than the diffusion length. Our results also suggest that growth of bulk n- or p-type GaAs under Ga-rich conditions would achieve the highest electron diffusion length due to the further reduction of the deep electron trapping center EL2 by melt stoichiometry.

In summary, as a result of MRDC's progress during the NASA program, 3-in. diameter n- and p-type LEC GaAs single crystals can be reproducibly grown with low dislocation densities and background impurities, high electrical mobilities, good dopant uniformities, and long diffusion lengths. On the basis of these excellent qualities, LEC material should be applicable to most solar cell applications. The capability for producing these large-area, high-quality substrates should positively impact the manufacturability of highly efficient, low-cost, and radiation-hard GaAs solar cells.

Finally, it is important to note that the low background impurity concentration in bulk LEC GaAs is extremely important for solar cells in which the substrate is passive, such as in a conventional "buffered" GaAs-GaAlAs heterostructure. In these devices, out-diffusion from the substrate to active regions of the device of fast-moving metallic impurities such as Fe, is detrimental to performance and radiation hardness, since these impurities act as carrier traps, reducing the minority carrier lifetime, and as compensation centers, changing the effective carrier concentration of the region in which

diffusion takes place. Lower levels of background impurities will result in fewer impurities reaching the active region of the device. Thus, adverse effects from out-diffusion are expected to be minimal with LEC GaAs.

6.0 REFERENCES

1. J.R. Oliver, R.D. Fairman, R.T. Chen and P.W. Yu, Elect. Lett. 17, 838 (1981).

2. D.E. Holmes, R.T. Chen, K.R. Elliot and C.G. Kirkpatrick, Appl. Phys. Lett. 40, 46 (1982).

3. D.E. Holmes, R.T. Chen, K.R. Elliot, C.G. Kirkpatrick and P.W. Yu, IEEE Trans. MMT-30, 949 (1982).

4. W.H. Hackett, Jr., J. Appl. Phys. 43, 1649 (1972).

5. C.C. Shen, K.P. Pande and G.L. Pearson, J. Appl. Phys. 53, 1236 (1982).

6. D.R. Wight, P.E. Oliver, T. Prentice and V.W. Steward, J. Crystal Growth 55, 183 (1981).

7. R.T. Chen and D.E. Holmes, J. Crystal Growth, 61, 111, (1983).

8. S. Uemura, S. Shinoyama, A. Yamamoto and S. Tohno, J. Crystal Growth 52, 591 (1981).

9. T. Suzuki, S.I. Akai, K. Kohe, Y. Hishida, K. Fujita and N. Kito, Sumitomo Elec. Tech. Rev. 18, 105 (1978).

10. Rasa Company, Japan, private communication.

11. W.G. Pfam, Trans. AIMA 194, 747 (1952).

12. J.B. Mullin, A. Royle and S. Benn, J. Crystal Growth 50, 625 (1980).

13. R.K. Willardson and W.P. Allred, Int. Symp. on GaAs, Reading, England, 1966, Inst. Phys. Conf., Ser. No. 3, p. 35.

14. J.R. Carruthers and K. Nassau, J. Appl. Phys. 39, 5205 (1968).

15. J. Burton, R. Prim and W. Slichter, J. Chem. Phys. 21, 1987 (1953).

16. K.R. Elliott, D.E. Holmes, R.T. Chen and C.G. Kirkpatrick, Appl. Phys. Lett. 40, 898 (1982).

17. A.M. Sekela, D.L. Feucht and A.G. Milnes, Inst. Phys. Conf., Ser. No. 24, 245 (1975).

18. H.C. Casey, B.I. Miller and E. Pinkas. J. Appl. Phys. 44, 1281 (1973).

19. T.S. Rao-Sahib and D.B. Wittry, J. Appl. Phys. 40, 3745 (1969).